ARTICLE

Nanocomposites of Vertically Aligned Single-Walled Carbon Nanotubes by Magnetic Alignment and Polymerization of a Lyotropic Precursor

Meagan S. Mauter, Menachem Elimelech, and Chinedum O. Osuji*

Department of Chemical and Environmental Engineering, Yale University, P.O. Box 208286, New Haven, Connecticut 06520-8286, United States

ABSTRACT We demonstrate a novel path for the fabrication of thin-film polymer nanocomposites containing vertically aligned single-walled carbon nanotubes (SWNTs). Liquid crystal mesophases of hexagonally packed cylindrical micelles orient with their long axes parallel to an applied magnetic field and template the alignment of SWNTs sequestered in the micellar cores. The mesophase is a stable single-phase material containing monomers that can be polymerized after nanotube alignment to form the nanocomposite polymer. The space-pervasive nature of magnetic fields and the tunable physicochemical properties of multicomponent mesophases make this an attractive approach that can be leveraged for application in diverse nanocomposite systems.

KEYWORDS: alignment · nanocomposite · single-walled carbon nanotube · SWNT · magnetic field · liquid crystal · thin-film

Many properties of polymer nanocomposites are determined by the anisotropy and orientation of the sequestered nanomaterials. In some cases, the anisotropy of the nanomaterial is useful only for the realization of an isotropic system property. For example, the bulk mechanical properties of polymer melts may be enhanced by the inclusion of high-aspect ratio nanoparticles, which have a lower percolation threshold than an equivalent mass of spherical nanoparticles.[1] In other cases, the anisotropy of the sequestered nanomaterial imparts "higher level" anisotropy in the bulk properties of the system. Controlled orientation of nanomaterial inclusions in polymer films produced demonstrations of anisotropic permeability,[1,2] thermal[3,4] and electrical[5,6] conductivity, enhanced mechanical properties,[7,8] and photovoltaic activity.[9,10]

Current methods for controlling orientation in nanocomposite materials, however, are limited by their effectiveness and scalability. In polymeric materials containing single-walled carbon nanotubes (SWNTs), mechanical shear,[11] anisotropic flow,[7,12] gel extrusion,[13] melt stretching,[14] magnetic fields,[15,16] and electric fields[17] have been used to varying effect to induce nanotube alignment. Despite these efforts, the fabrication of aligned SWNT-polymer nanocomposite matrices remains difficult, particularly in thin-film geometries where vertical alignment of the SWNTs in polymer films is attractive for applications in size and chemoselective transport.[18,19]

We propose a general route for the facile and scalable synthesis of polymeric nanocomposites containing oriented nanomaterials. The concept is outlined schematically in Figure 1. Magnetically aligned liquid crystalline (LC) mesophases formed by surfactants act as structure-directing templates for the alignment of sequestered nanomaterials. The surfactant mesophase is polymerizable, either inherently due to the structure of the surfactant, or *via* the incorporation of a monomeric species in the formulation of the mesophase. The slow relaxation of lyotropic phases preserves nanomaterial orientation until post-alignment photopolymerization of the system forms the nanocomposite support matrix. The space-pervasive nature of magnetic fields enables simple control over orientation, provides excellent compatibility with thin-film geometries, and is inherently scalable to macroscopic dimensions exceeding several centimeters. Furthermore, the chemical diversity of species capable of forming lyotropic mesophases provides a rich parameter space for addressing issues related to nanomaterial dispersion, functionalization, and monomer/polymer compatibility. This synthesis route may find application in reinforced polymeric materials, solar cells, or aligned carbon nanotube membranes.

*Address correspondence to chinedum.osuji@yale.edu.

Received for review August 16, 2010 and accepted October 06, 2010.

Published online October 18, 2010.
10.1021/nn102047j

© 2010 American Chemical Society

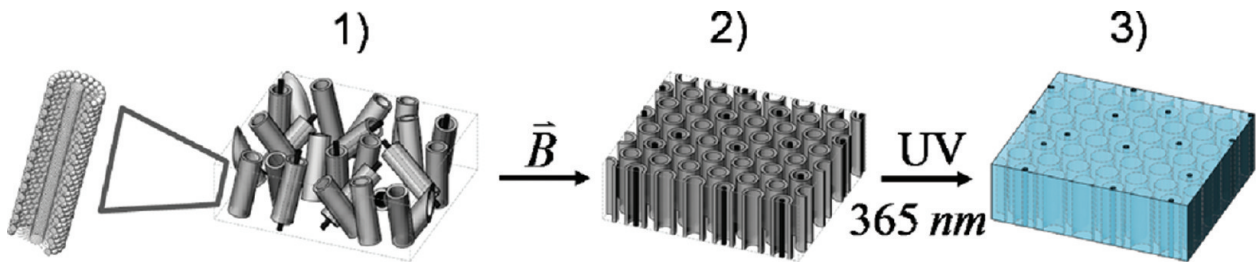

Figure 1. Proposed scheme for the fabrication of vertically aligned SWNT polymer nanocomposite thin-film: (1) sequestration of SWNT into cylindrical micelle mesophase; (2) magnetic field alignment of cylindrical micelles; (3) polymerization of mesophase to form a polymer thin-film embedded with vertically aligned SWNT.

Magnetic field alignment of materials is driven by anisotropy of magnetic susceptibility, expressed coherently on a length scale sufficient to create a free energy difference between aligned and unaligned states that is significant with respect to thermal energy, kT. In this respect, magnetic alignment is analogous to electric field alignment. The magnetic free energy difference ΔF_M scales as $\Delta\chi B^2$, where $\Delta\chi$ is the anisotropy of magnetic susceptibility and B is the field strength, whereas the electric free energy ΔF_E scales as $\Delta\varepsilon E^2$, where $\Delta\varepsilon$ is the anisotropy of dielectric permittivity and E the field strength. In practical application, however, magnetic fields possess a number of advantages over electric fields. The space-pervasive nature of magnetic fields, the absence of electrode contact issues, and the independence from dielectric breakdown concerns allow for magnetic alignment of diamagnetically anisotropic materials without severe constraints on the geometry or form factor of the system.[20]

For nanocomposite systems with low intrinsic anisotropy or small correlation volumes, direct magnetic alignment requires field strengths that are impractical for commercial processes. Direct alignment of nanotubes requires magnetic field strengths between 10 and 35 T,[21,22] depending on the chirality and diameter of the SWNTs,[23] due to the large competing effect of thermal forces on the single tube length scale.[24] One convenient alternative is to template the alignment of the nanomaterial *via* sequestration in an appropriate lyotropic or thermotropic mesophase, which can be aligned at lower field strengths of 1−5 T. The alkyl tails of prototypical ionic surfactants, such as dodecyltrimethylammonium bromide and sodium dodecyl sulfate, and of nonionics such as Brij possess a negative diamagnetic anisotropy and align perpendicularly to an applied magnetic field.[25,26] Self-assembly of the surfactant molecules into cylindrical micelles imparts a positive diamagnetic anisotropy to the micelle as a whole, due to the orthogonality of the alkyl tail to the long axis of the cylindrical structure. Thus, in the hexagonal or H_I phase, the long axes of the hexagonally packed cylindrical micelles orient parallel to the applied magnetic field.[27−29]

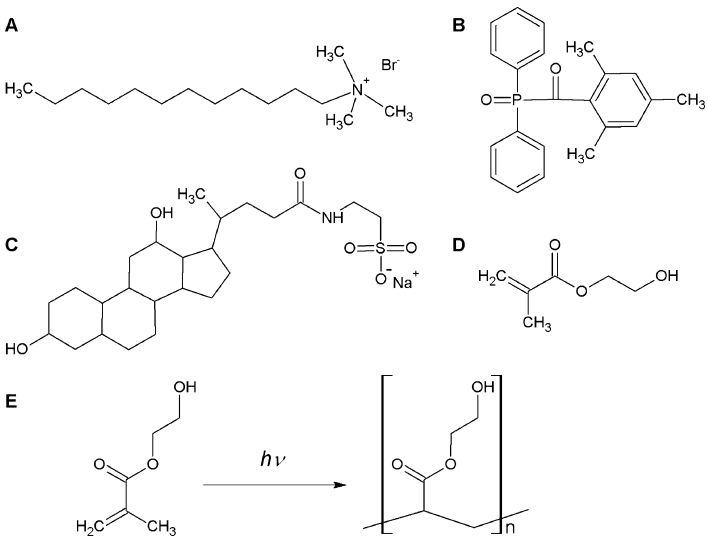

Figure 2. Chemical structures of (A) hydroxyethylmethacrylate (HEMA); (B) sodium taurodeoxycholate (TDOC); (C) dodecyltrimethylammonium bromide (DTAB); (D) Photoinitiator Darocure TPO (Ciba Specialty Chemicals). (E) Polymerization reaction of HEMA to form poly(hydroxyethylmethacrylate).

In a nanocomposite mesophase containing anisotropic nanomaterials, the free energy minimum is produced by parallel alignment of the nanomaterials with respect to the mesophase director field, as this arrangement minimizes elastic distortions of the mesophase. Sequestration of SWNTs within the mesophase template thus enables nanotube alignment concurrent with the alignment of the mesophase.[15] The final consideration in mesophase alignment is the kinetic limitation to mesogen orientation. While the thermodynamic preference for materials with positive diamagnetic anisotropy is to align parallel to the applied magnetic field, the slow kinetics in viscous systems can prolong the LC matrix in a nonequilibrium, unaligned state. Efficient or rapid alignment of the mesophase is enabled by the imposition of the magnetic field during the thermally driven disorder-to-order transition of the system. In the vicinity of this transition temperature, T_{ODT}, the evolution of the structure is strongly coupled to alignment as ordered material nucleates in the presence of the field and the thermally enhanced mobility of the system facilitates fast alignment.

Here, we report on the phase behavior and alignment of a stable single-phase multicomponent system that simultaneously forms the required anisotropic lyotropic mesophase and supports the inclusion of polymerizable species. Importantly, the system possesses a

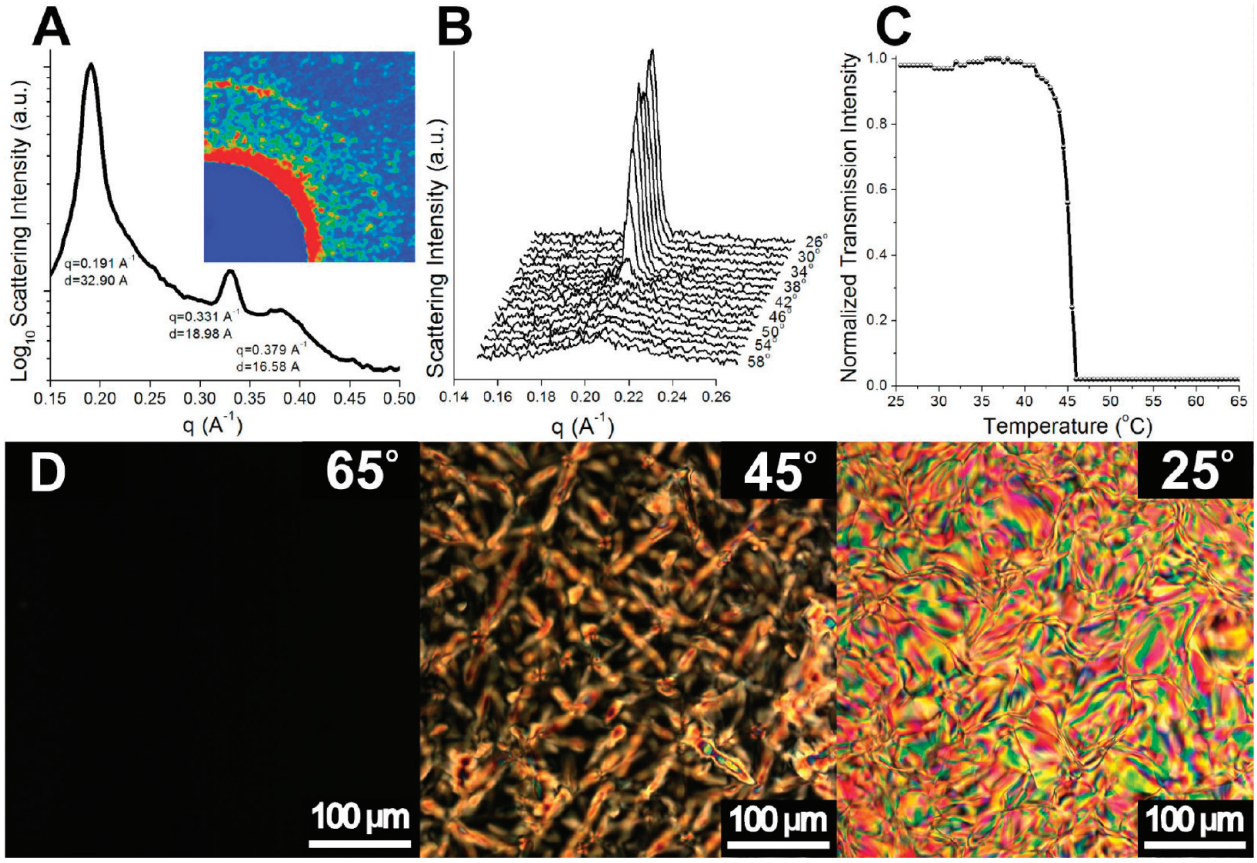

Figure 3. Phase behavior of stable mesophase. (A) Scattering intensity *versus* scattering vector plotted from WAXS demonstrates hexagonal packing of cylindrical micelles in the mesophase; (inset A) 2D scattering from WAXS image plate; (B) temperature dependent SAXS confirms temperature region of order−disorder transition; (C) transmitted intensity of polarized light as a function of temperature illustrates order−disorder transition at 45 °C; (D) polarized optical micrographs depicting liquid crystalline texture of the mesophase as a function of temperature.

thermally accessible order−disorder transition to facilitate rapid alignment, and the system also includes dispersants to stabilize nanotubes against aggregation. Magnetic field strengths as low as a few Tesla direct the alignment of hexagonally packed cylindrical micelles on time scales less than 1 h, and these micelles template the alignment of the sequestered carbon nanotubes. Polymerization of the mesophase by exposure to 365 nm UV light produces a mechanically robust polymer film that maintains the aligned structure imposed by the magnetic field on the precursor phase. We show that this approach can be used to fabricate polymer films in which SWNTs are aligned with their long axes perpendicular to the film surface.

RESULTS AND DISCUSSION

We sequester and align SWNTs within a stable lyotropic LC mesophase composed of surfactant dodecyltrimethylammonium bromide (DTAB), monomer hydroxyethyl methacrylate (HEMA), solvent (water), cross-linker poly(ethylene glycol)-400 dimethacrylate, and photoinitiator Darocure TPO (Figure 2). A systematic survey of the phase behavior of our multicomponent system was conducted as a function of temperature and composition. Polarized optical microscopy (Zeiss Axiovert 200 M with crossed polarizers) was used to record textures of birefringent samples and X-ray scattering (Rigaku S-MAX 3000 with 2D small-angle (SAXS) and wide-angle (WAXS) detectors) was used to characterize periodicities for phase identification. We isolated the H_I phase space by using a polarized optical microscope at room temperature to categorize LC textures. X-ray scattering revealed the characteristic 1:3:4 ratios of the square of scattering vector peak locations seen for hexagonally packed structures (Figure 2A). The primary reflection was at $q = 0.191$ Å^{-1}, corresponding to a *d*-spacing of 3.3 nm and a cylinder-to-cylinder spacing of 3.7 nm.

Temperature dependent SAXS was used to determine T_{ODT} from the decay of the primary scattering peak of the hexagonal structure with increasing temperature. A smooth, hysteresis-free transition from the hexagonally packed H_I phase to a disordered micellar phase occurs around 42 °C (Figure 3B). This is confirmed by temperature-dependent optical microscopy in which a plot of transmitted light intensity as a function of temperature displays an ODT near 45 °C (Figure 3C,D). This relatively low temperature, with respect to the boiling point of the solvent (water), affords a nontrivial benefit over the use of surfactants such as sodium dodecyl sulfate, which do not display a thermally acces-

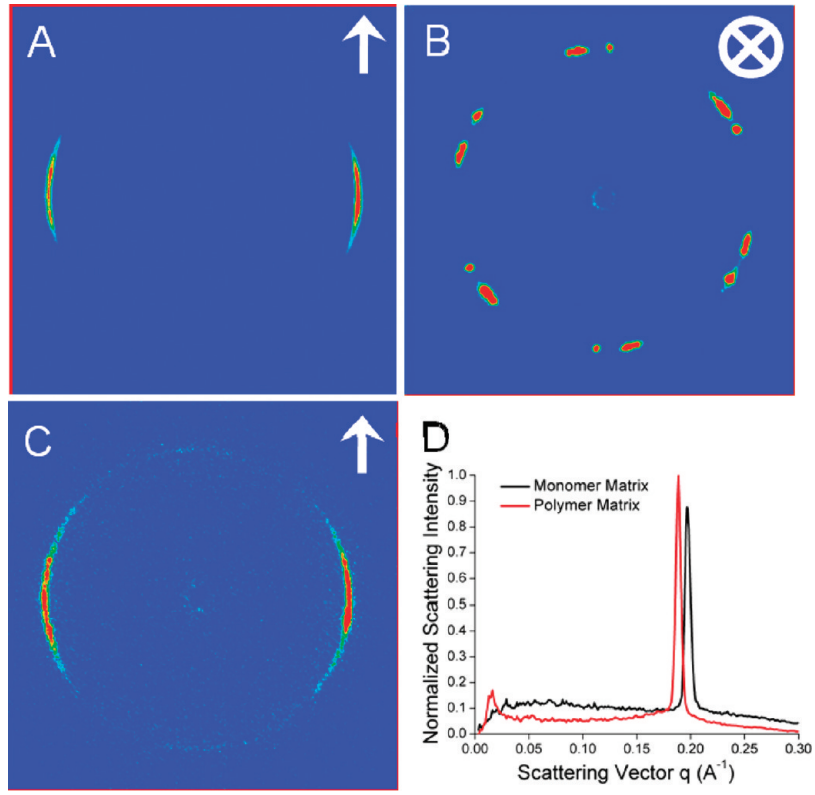

Figure 4. SAXS patterns of pre- and postpolymerized aligned samples. The arrows and cross indicate the direction of the applied magnetic field in the plane and out of the plane, respectively: (A) in-plane alignment of sample before polymerization; (B) out-of-plane alignment of sample before polymerization; (C) scattering from in-plane aligned sample after polymerization shows that the system retains its alignment after polymerization of the host matrix; (D) integrated SAXS data show that the pre- and post-polymerized samples have similar *d*-spacings of 3.2 and 3.3 nm, respectively.

sible clearing temperature in aqueous lyotropic assemblies. The phase boundary at 42 °C enables facile, complete, and rapid alignment of the host matrix when slowly cooled across this transition under the applied field. In the absence of the field, however, the matrix is sufficiently viscous at room temperature to preserve alignment during characterization and subsequent polymerization of the gel. These are crucial features of the multicomponent system for the efficient realization of magnetically aligned nanocomposites.

Prior work on the phase behavior of binary lyotropic mesophases consisting of DTAB and water identified the existence of an H_I phase between 56% and 73% DTAB by weight, and a coexistent region of hexagonal and micellar phases between 56% and 20% (w/w).[30] No order−disorder transition was reported for the H_I phase on increasing temperatures up to the boiling point of the solvent (water) at 100 °C. The phase behavior of the ternary DTAB, HEMA, and water system explored in this work differs from the phase behavior of the binary system in two critical aspects. First, the ternary system possesses an order−disorder transition at moderate temperatures (<50 °C) between a birefringent hexagonal phase and a non-birefringent isotropic micellar phase. Second, the H_I phase of the ternary system is shifted to lower DTAB concentrations. One of the critical drawbacks in the utilization of lyotropic surfactant mesophases is the typically large volume fraction occupied by the surfactant in the system. In the H_I phase of the binary DTAB and water system, for example, the surfactant can account for up to 73% of the total volume, leaving only 27% of the phase space available for a solvent phase that serves as a vehicle for introducing the nanomaterial. The shift of the H_I phase to lower DTAB concentrations in the ternary system increases the volume of the system available for the inclusion of other functional components. The phase behavior observed here is consistent with that reported for amphiphilic cationic monomers based on DTAB.[31]

An ideal structure directing mesophase should exhibit both strong diamagnetic anisotropy of susceptibility and efficient dispersion of the nanomaterial. In the present work, alignment of the nanotubes is enabled by their sequestration into the micellar cores of the diamagnetically anisotropic DTAB cylindrical micelles. The alkyl tails of the surfactant adsorb to the hydrophobic SWNTs to simultaneously disrupt the van der Waals attractive forces between SWNTs and confine the individual nanotubes within the cylindrical micelles.[32] Enthalpically favorable interaction between the nanotube and the cylindrical micelle couples the orientation of these two uniaxial species, such that alignment of the SWNTs results from alignment of their confining mesophase structures. The dispersion of the nanotubes,

that is, their stabilization in the micellar cores, represents a secondary role for the surfactant molecules comprising the host matrix. The efficiency with which the surfactant disperses the nanotubes in solution enforces a limit on the density of single dispersed SWNT in the final nanocomposite. In the present system, we overcame the limited efficacy of DTAB as a dispersing agent by first debundling the SWNTs in a 1% solution of sodium taurodeoxycholate (TDOC) (Supporting Information, Figure S1). The sharp absorbance peaks (van Hove singularities) of the near-IR spectra at 785 nm excitation wavelength suggest effective dispersion of the SWNTs[33,34] in the TDOC solution and the supporting matrix, though other researchers have also employed small angle neutron scattering (SANS) as a metric for quantifying SWNT dispersion.[35] In lieu of SANS experiments, we further corroborated SWNT dispersion by comparing transmission electron microscopy (TEM) images before and after the surfactant-aided debundling of the SWNTs (Supporting Information, Figure S2).

Alignment was conducted in a superconducting magnet with tunable static field strength up to 6 T (AMI - American Magnetics, Inc.). The magnet features orthogonal room-temperature bores, one of which housed the apparatus for these experiments. The sample chamber is isolated from the ambient conditions of the bore and is temperature controlled to ± 0.1 °C for precise thermal treatment of samples. Material was loaded at room temperature into circular sample cells 1−2 mm thick and 5 mm in diameter. To perform alignment, the composite mesophase was heated above its order−disorder transition temperature into the isotropic micellar phase, and slowly cooled at 0.5 °C/min back into the H_I phase in the presence of a 5 T field.

After alignment, the sample holder was transferred from the magnet to the SAXS instrument for characterization of the mesophase alignment. Two-dimensional SAXS patterns demonstrate controlled in-plane and out-of-plane alignment of the system. In Figure 4A, the concentration of the scattered intensity along the equatorial direction indicates that the cylindrical micelles are aligned with their long axes along the field direction, which is indicated by the arrow. In Figure 4B, data are presented for the same sample after physical rotation and realignment in the field. The scattering plane is now perpendicular to the field line. The image shows two 6-fold symmetric patterns, indicating that there are contributions from 2 large grains with slightly different angular orientations in-plane, with the hexagonally packed cylinders aligned along the field direction. The X-rays sample a region roughly 0.5 mm in diameter, so the alignments produced here are coherent over that length scale. Polarized optical microscopy was also used to confirm the production of large area monodomains (Figure 5).

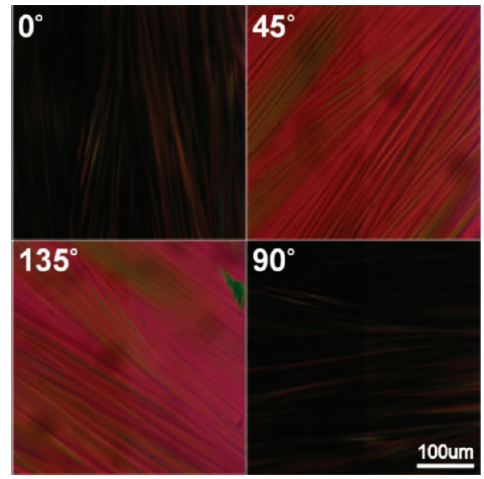

Figure 5. Angle-dependent polarized optical micrographs of aligned system showing near uniform extinction and passage of light over large areas.

The aligned samples were polymerized by exposure to UV light (365 nm) to form a poly(hydroxylethyl methacrylate) polymer film containing surfactant-coated aligned SWNTs. Crucially, the alignment and periodicity of the mesostructure in the polymer film are unchanged relative to those of the lyotropic precursor. The 2-D SAXS pattern taken from the polymerized sample shows a well maintained alignment of structures along the field direction (Figure 4C). The primary reflection is at $q = 0.189$ Å^{-1}, corresponding to a *d*-spacing of 3.3 nm, which is only slightly increased relative to the 3.2 nm of the hexagonally ordered precursor (Figure 4D). The film produced is mechanically robust and has a clear, uniform appearance (Figure 6).

X-ray scattering cannot provide a viable measure of nanotube alignment here due to the low concentration of nanotubes and limited electron density contrast between the SWNTs and the host mesophase. Instead, polarized Raman spectroscopy was used to provide a statistically relevant indication of SWNT alignment within the polymer nanocomposite. The distinct Raman modes of the SWNT and host matrix (Figure 7A) were used to assess alignment using polarized Raman spectroscopy.

SWNTs display characteristic peaks at Raman shifts of 1350 and 1590 cm^{-1}, corresponding to the first order peaks of amorphous carbon and 2-D graphite, respectively. These Raman modes show maximum intensity

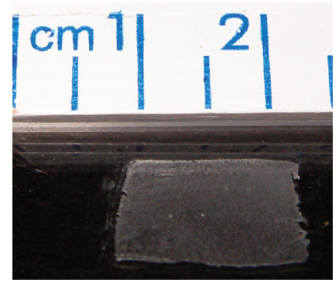

Figure 6. Polymer film containing vertically aligned SWNT. Film thickness is roughly 1 mm.

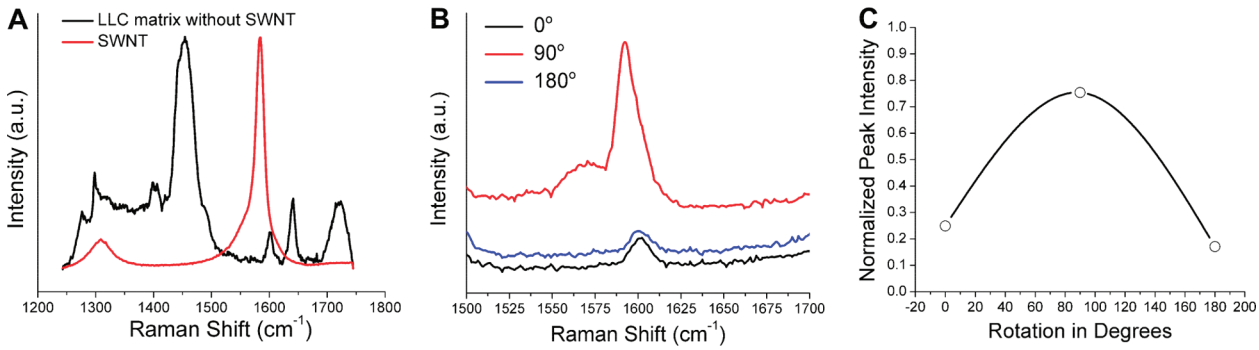

Figure 7. (A) Nonpolarized Raman spectroscopy of SWNT and the host mesophase; (B) Polarized Raman spectroscopy of aligned nanocomposite material; (C) normalized peak intensity calculated from the magnitude of the characteristic G band peak (1590 cm^{-1}) for SWNT and normalized to average baseline intensity between 1510 and 1540 cm^{-1}.

when the polarization of the incident radiation (electric field oscillation) is parallel to the nanotube long axis, such that a matrix of aligned SWNTs will exhibit peak-to-valley variations in the Raman intensity as the sample is rotated in 90° increments.[36] At 0°, or when the long-axis of the nanotube is perpendicular to the polarization of the excitation laser's oscillating electromagnetic field, the Raman scattering from the SWNTs should display a minimum. At 90°, however, the Raman signal intensity of the SWNT peaks is maximized due to enhanced absorption, molecular polarization, and optical conductivity along the long-axis of the nanotube.[37] Rotation of the sample by a further 90° should result in a drastically reduced signal as the SWNT long axes again become orthogonal to the direction of electric field oscillation of incident light. This is precisely what is observed. Raman scattering intensities were recorded at three sample orientations, spaced by 90°, with respect to the polarization of incident light (Figure 7B,C). The variation in Raman signal intensity was considered by appropriate normalization of the SWNT peak at 1590 cm^{-1} to the baseline average between 1525 and 1550 cm^{-1}.

CONCLUSION

We have demonstrated a facile method for the fabrication of a vertically aligned SWNT composite film using magnetic field aligned polymerizable lyoptropic surfactant mesophases as structure directing templates. X-ray scattering was used to characterize the field-guided assembly process, and polarized Raman spectroscopy demonstrated alignment of the SWNTs. The present approach could be of broad utility in applications ranging from membrane synthesis to photovoltaics, where aligned nanomaterials and periodic interfaces play a key role in determining the properties of the system.

MATERIALS AND METHODS

Preparation of Lyotropic Matrix. A stable lyotropic LC mesophase is formed of 47.5% dodecyltrimethylammonium bromide (Sigma-Aldrich, St. Louis, MO), 33% deionized water, 18% hydroxyethyl methacrylate (Sigma-Aldrich, St. Louis, MO), 1% poly(ethylene glycol)-400 dimethacrylate (Sigma-Aldrich, St. Louis, MO), and 0.5% Darocure TPO (Ciba, Basel, Switzerland). The sequestered nanomaterials, in this case single-walled carbon nanotubes (SWNTs), are introduced to the system *via* dispersal in the aqueous phase.

To facilitate this dispersion we prepare a 1% sodium taurodeoxycholate hydrate solution initially containing 1 g/L SWNTs prepared by CO disproportionation over highly dispersed cobalt substituted MCM-41 and an amorphous silica catalyst at 600 °C. The solution is suspended in an ice bath and probe sonicated for 1 h. After sonication, the solution is centrifuged in a Sorvall RC 6+ Centrifuge (Thermo Fisher, Waltham, MA) at 25000*g* for 1 h to separate aggregated SWNTs. In the event of persistent aggregation, the sonication and centrifugation procedure is repeated. The solution visibly decreases in SWNT density, but the near-infrared data demonstrate singly dispersed SWNTs at the conclusion of this procedure (Supporting Information, Figure S1). Details on the SWNT diameter and chirality are published elsewhere,[38] but, on average, the SWNT samples were 93% semiconducting and 7% metallic. The dispersed SWNTs are substituted for deionized water in the preparation of the mesophase−SWNT nanocomposite. Dispersion was maintained across the range of weight percent SWNT in matrix that we tested, approximately 0.028%−0.076% (Supporting Information, Figure S3). The effects of 0.33% of TDOC on the phase behavior of the LC mesophase were undetectable.

Magnetic Alignment of LC Mesophase. Aligned LC mesophase samples were prepared in both thin-film (roughly 0.1−0.25 mm thickness) and bulk (1−3 mm thickness) geometries. The alignment and phase behavior between the two sample geometries were consistent, demonstrating that surface effects were undetectable or otherwise negligible in our experiment. Alignment was conducted in a superconducting magnet with tunable static field strength up to 6 T (American Magnetics, Oak Ridge, TN). The temperature of the samples in the magnetic field is manipulated through a programmable temperature controller (Omega, Stamford, CT) that provides temperature control within 0.1 °C of set points. The LC mesophase is heated to 65 °C and held at that temperature for 1 min before cooling through T_{ODT} to 35 °C at a rate of 0.5 °C/min. Two hours of sample annealing under the field between 30 and 35 °C further improved the orientational order in the system. Alignment of the mesophase is confirmed *via* X-ray scattering on a Rigaku S-MAX 3000 (Tokyo, Japan) with 2D small-angle (SAXS) and wide-angle (WAXS) detectors.

Polymerization. The aligned mesophase is polymerized under a 365 nm ultraviolet lamp with an intensity of 500 $\mu W/cm^2$ (UVP, Upland, CA).

Polarized Raman Spectroscopy. The alignment of sequestered SWNTs is determined using a Renishaw inVia confocal Raman microscope (Renishaw, Gloucestershire, United Kingdom) equipped with a polarizer and a half wave plate for orientational analysis. Using an excitation wavelength of 488 nm, we ob-

tain the Raman shift of the sample over the region of interest from 1250 to 1750 cm^{-1} at sample rotations of 0°, 90°, and 180°. The variation in Raman signal intensity of the characteristic graphene (G) band peak at 1590 cm^{-1} is considered by appropriate normalization of the G-band peak intensity to the average baseline intensity between 1525 and 1550 cm^{-1}.

Acknowledgment. The authors thank L. Pfefferle and members of her lab for advice and assistance in nanotube fabrication and characterization. M.S.M. acknowledges generous support from the AWWA Abel Wolman Fellowship, the NSF Graduate Research Fellowship Program (GRFP), and the EPA Science to Achieve Results (STAR) Graduate Fellowship Program. C.O.O. acknowledges NSF support under DMR-0847534. M.E. acknowledges the support of WaterCAMPWS, an STC of Advanced Materials for the Purification of Water with Systems under the NSF Grant CTS-0120978.

Supporting Information Available: Near infrared spectra (Figure S1), TEM images of debundled SWNT (Figure S2), and images of the composite matrix with varying concentrations of SWNTs (Figure S3). This material is available free of charge *via* the Internet at http://pubs.acs.org.

REFERENCES AND NOTES

1. Pike, G. E.; Seager, C. H. Percolation and Conductivity: A Computer Study. I. *Phys. Rev. B* **1974**, *10*, 1421.
2. Holt, J. K.; Park, H. G.; Wang, Y.; Stadermann, M.; Artyukhin, A. B.; Grigoropoulos, C. P.; Noy, A.; Bakajin, O. Fast Mass Transport through Sub-2-Nanometer Carbon Nanotubes. *Science* **2006**, *312*, 1034–1037.
3. Choi, E. S.; Brooks, J. S.; Eaton, D. L.; Al-Haik, M. S.; Hussaini, M. Y.; Garmestani, H.; Li, D.; Dahmen, K. Enhancement of Thermal and Electrical Properties of Carbon Nanotube Polymer Composites by Magnetic Field Processing. *J. Appl. Phys.* **2003**, *94*, 6034–6039.
4. Moniruzzaman, M.; Winey, K. I. Polymer Nanocomposites Containing Carbon Nanotubes. *Macromolecules* **2006**, *39*, 5194–5205.
5. Du, F.; Fischer, J. E.; Winey, K. I. Effect of Nanotube Alignment on Percolation Conductivity in Carbon Nanotube/Polymer Composites. *Phys. Rev. B* **2005**, *72*, 121404.
6. Sandler, J. K. W.; Kirk, J. E.; Kinloch, I. A.; Shaffer, M. S. P.; Windle, A. H. Ultralow Electrical Percolation Threshold in Carbon-Nanotube−Epoxy Composites. *Polymer* **2003**, *44*, 5893–5899.
7. Haggenmueller, R.; Gommans, H. H.; Rinzler, A. G.; Fischer, J. E.; Winey, K. I. Aligned Single-Wall Carbon Nanotubes in Composites by Melt Processing Methods. *Chem. Phys. Lett.* **2000**, *330*, 219–225.
8. Thostenson, E. T.; Chou, T. W. Aligned Multiwalled Carbon Nanotube-Reinforced Composites: Processing and Mechanical Characterization. *J. Phys. D* **2002**, *35*, L77–L80.
9. Ahir, S. V.; Huang, Y. Y.; Terentjev, E. M. Polymers with Aligned Carbon Nanotubes: Active Composite Materials. *Polymer* **2008**, *49*, 3841–3854.
10. Kang, Y.; Kim, D. Well-Aligned CdS Nanorod Conjugated Polymer Solar Cells. *Sol. Energy Mater. Sol. Cells* **2006**, *90*, 166–174.
11. Jin, L.; Bower, C.; Zhou, O. Alignment of Carbon Nanotubes in a Polymer Matrix by Mechanical Stretching. *Appl. Phys. Lett.* **1998**, *73*, 1197–1199.
12. Kim, S.; Jinschek, J. R.; Chen, H.; Sholl, D. S.; Marand, E. Scalable Abrication of Carbon Nanotube/Polymer Nanocomposite Membranes for High Flux Gas Transport. *Nano Lett.* **2007**, *7*, 2806–2811.
13. Vigolo, B.; Penicaud, A.; Coulon, C.; Sauder, C.; Pailler, R.; Journet, C.; Bernier, P.; Poulin, P. Macroscopic Fibers and Ribbons of Oriented Carbon Nanotubes. *Science* **2000**, *290*, 1331–1334.
14. Fagan, J. A.; Simpson, J. R.; Landi, B. J.; Richter, L. J.; Mandelbaum, I.; Bajpai, V.; Ho, D. L.; Raffaelle, R.; Walker, A. R. H.; Bauer, B. J.; Hobbie, E. K. Dielectric Response of Aligned Semiconducting Single-Wall Nanotubes. *Phys. Rev. Lett.* **2007**, *98*, 147402.
15. Lagerwall, J.; Dettlaff-Weglikowska, S.; Roth, F.; Scalia, G.; Haluska, M.; Giesselmann, F. Nanotube Alignment Using Lyotropic Liquid Crystals. *Adv. Mater.* **2007**, *19*, 359–364.
16. Walters, D. A.; Casavant, M. J.; Qin, X. C.; Huffman, C. B.; Boul, P. J.; Ericson, L. M.; Haroz, E. H.; O'Connell, M. J.; Smith, K.; Colbert, D. T.; Smalley, R. E. In-Plane-Aligned Membranes of Carbon Nanotubes. *Chem. Phys. Lett.* **2001**, *338*, 14–20.
17. Park, C.; Wilkinson, J.; Banda, S.; Ounaies, Z.; Wise, K. E.; Sauti, G.; Lillehei, P. T.; Harrison, J. S. Aligned Single-Wall Carbon Nanotube Polymer Composites Using an Electric Field. *J. Polym. Sci., Part B* **2006**, *44*, 1751–1762.
18. Majumder, M.; Chopra, N.; Hinds, B. J. Effect of Tip Functionalization on Transport through Vertically Oriented Carbon Nanotube Membranes. *J. Am. Chem. Soc.* **2005**, *127*, 9062–9070.
19. Lopez-Lorente, A. I.; Simonet, B. M.; Valcarcel, M. The Potential of Carbon Nanotube Membranes for Analytical Separations. *Anal. Chem.* **2010**, *82*, 5399–5407.
20. Osuji, C.; Ferreira, P. J.; Mao, G. P.; Ober, C. K.; Vander Sande, J. B.; Thomas, E. L. Alignment of Self-Assembled Hierarchical Microstructure in Liquid Crystalline Diblock Copolymers Using High Magnetic Fields. *Macromolecules* **2004**, *37*, 9903–9908.
21. Shaver, J.; Parra-Vasquez, A. N. G.; Hansel, S.; Portugall, O.; Mielke, C. H.; von Ortenberg, M.; Hauge, R. H.; Pasquali, M.; Kono, J. Alignment Dynamics of Single-Walled Carbon Nanotubes in Pulsed Ultrahigh Magnetic Fields. *ACS Nano* **2009**, *3*, 131–138.
22. Smith, B. W.; Benes, Z.; Luzzi, D. E.; Fischer, J. E.; Walters, D. A.; Casavant, M. J.; Schmidt, J.; Smalley, R. E. Structural Anisotropy of Magnetically Aligned Single Wall Carbon Nanotube Films. *Appl. Phys. Lett.* **2000**, *77*, 663–665.
23. Searles, T. A.; Imanaka, Y.; Takamasu, T.; Ajiki, H.; Fagan, J. A.; Hobbie, E. K.; Kono, J. Large Anisotropy in the Magnetic Susceptibility of Metallic Carbon Nanotubes. *Phys. Rev. Lett.* **2010**, *105*, 017403.
24. Ajiki, H.; Ando, T. Magnetic Properties of Carbon Nanotubes. *J. Phys. Soc. Jpn.* **1993**, *62*, 2470–2480.
25. Majewski, P. W.; Osuji, C. O. Nondegenerate Magnetic Alignment of Self-Assembled Mesophases. *Soft Matter* **2009**, *5*, 3417–3421.
26. Shao, H. H.; Gang, H.; Sirota, E. B. Magnetic-Field Induced Orientation and Anisotropic Susceptibility of Normal Alkanes. *Phys. Rev. E* **1998**, *57*, R6265.
27. Clawson, J. S.; Holland, G. P.; Alam, T. M. Magnetic Alignment of Aqueous CTAB in Nematic and Hexagonal Liquid Crystalline Phases Investigated by Spin-1 NMR. *Phys. Chem. Chem. Phys.* **2006**, *8*, 2635–2641.
28. Firouzi, A.; Schaefer, D. J.; Tolbert, S. H.; Stucky, G. D.; Chmelka, B. F. Magnetic-Field-Induced Orientational Ordering of Alkaline Lyotropic Silicate Surfactant Liquid Crystals. *J. Am. Chem. Soc.* **1997**, *119*, 9466–9477.
29. Rapp, A.; Ermolaev, K.; Fung, B. M. The Alignment of Lyotropic Liquid Crystals Formed by Hexadecyltrimethylammonium Bromide in D_2O in a Magnetic Field. *J. Phys. Chem. B* **1999**, *103*, 1705–1711.
30. McGrath, K. M. Phase Behavior of Dodecyltrimethylammonium Bromide/Water Mixtures. *Langmuir* **1995**, *11*, 1835–1839.
31. Lester, C. L.; Guymon, C. A. Ordering Effects on the Photopolymerization of a Lyotropic Liquid Crystal. *Polymer* **2002**, *43*, 3707–3715.
32. Wenseleers, W.; Vlasov, I.; Goovaerts, E.; ED, O.; AS, L.; A, B. Efficient Isolation and Solubilization of Pristine Single-Walled Nanotubes in Bile Salt Micelles. *Adv. Funct. Mater.* **2004**, *14*, 1105–1112.
33. Chatterjee, T.; Yurekli, K.; Hadjiev, V. G.; Krishnamoorti, R. Single-Walled Carbon Nanotube Dispersions in Poly(Ethylene Oxide). *Adv. Funct. Mater.* **2005**, *15*, 1832–1838.
34. Saito, R.; Dresselhaus, G.; Dresselhaus, M. S. *Physical*

Properties of Carbon Nanotubes; Imperial College: London, 1998.
35. Fagan, J. A.; Landi, B. J.; Mandelbaum, I.; Simpson, J. R.; Bajpai, V.; Bauer, B. J.; Migler, K.; Hight Walker, A. R.; Raffaelle, R.; Hobbie, E. K. Comparative Measures of Single-Wall Carbon Nanotube Dispersion. *J. Phys. Chem. B* **2006**, *110*, 23801–23805.
36. Duesberg, G. S.; Loa, I.; Burghard, M.; Syassen, K.; Roth, S. Polarized Raman Spectroscopy on Isolated Single-Wall Carbon Nanotubes. *Phys. Rev. Lett.* **2000**, *85*, 5436 LP–5439.
37. Ajiki, H.; Ando, T. Aharonov−Bohm Effect in Carbon Nanotubes. *Phys. B* **2004**, *201*, 349–352.
38. Zoican Loebick, C.; Podila, R.; Reppert, J.; Chudow, J.; Ren, F.; Haller, G. L.; Rao, A. M.; Pfefferle, L. D. Selective Synthesis of Subnanometer Diameter Semiconducting Single-Walled Carbon Nanotubes. *J. Am. Chem. Soc.* **2010**, *132*, 11125–11131.